



Research paper

Estimation of actual evapotranspiration using the simplified-surface energy balance index model over an irrigated agricultural farm

TRIDIV GHOSH¹, BAPPA DAS², VINAY K SEHGAL¹, DEBASISH ROY³, JOYDEEP MUKHERJEE¹, RAJKUMAR DHAKAR¹, KUSHIK BAG⁴ and DEBASHIS CHAKRABORTY^{1*}

¹Division of Agricultural Physics, ICAR-Indian Agricultural Research Institute, New Delhi, India

²ICAR-Central Coastal Agricultural Research Institute, Old Goa-403402, Goa, India

³India Meteorological Department, New Delhi, India

⁴ICAR-Research Complex for NEH Region, Umiam, Meghalaya, India

* Corresponding author, EMAIL: debashisiari@gmail.com

ABSTRACT

Evapotranspiration (ET) plays a crucial role in the energy and water balance of agricultural ecosystems and is a vital component of the hydrological cycle. Efficient irrigation water management relies on accurate spatiotemporal coverage of crop ET across a farm. Thanks to the availability of multi-temporal high-resolution satellite datasets and remote sensing-based surface energy balance models, near-real-time estimation of ET is now possible. This study utilized Landsat 8/9 data to estimate ET using the simplified surface energy balance index (S-SEBI) model, which was then compared to eddy covariance measurements over a semi-arid agricultural farm in New Delhi, India during the post-monsoon periods of 2021-22 and 2022-23. The S-SEBI model predicted daily ET from Landsat 8/9 data with an average correlation coefficient and RMSE of 0.89 and 0.79 mm/day, respectively. The spatiotemporal map was also used to evaluate the model's performance, and it could accurately differentiate between ET over dryland crops and well-irrigated wheat fields on the farm. Despite underestimating ET (0.51 mm/day) during the initial growing season (Nov-Dec) and overestimating it (0.73 mm/day) during mid-season (Feb-Mar), the S-SEBI model can still be an operational tool for mapping ET with high accuracy and sufficient variation across pixels, making it an ideal option for incorporating into irrigation scheduling.

Keywords: Evapotranspiration, S-SEBI, Eddy Covariance, Land Surface Temperature

Global population growth, climate change, competition from other uses, and increased regulation of agricultural water use are causing water to become increasingly scarce (Boretti and Rosa, 2019; Kisekka *et al.*, 2022). So, advanced technologies are required to optimize water use in agriculture urgently. Evapotranspiration (ET), as an essential part of crop water use, has several agricultural, climatological, and hydrological applications like estimating crop water stress, surface runoff, irrigation scheduling, drought management, and water budget analysis (Cleverly *et al.*, 2015; Sholihah *et al.*, 2016; Bag *et al.*, 2020; Kumar *et al.*, 2020). Conventional methods, such as lysimeters, eddy covariance systems, Bowen ratio energy balance (BREB), and tower flux, though they provide ET estimates at higher accuracy based on local meteorological data, are point-based strategies rather than an assessment of spatial ET distribution (Jin *et al.*, 2018).

Remote sensing (RS) offers a relatively frequent and spatially contiguous means of tracking surface biophysical parameters that influence ET, such as albedo, vegetation type, and density, on a global scale (Parmar and Gontia, 2016; Pimpale *et al.*, 2015; Chattopadhyay *et al.*, 2016). ET mapping based on RS is a low-cost method of estimating and monitoring this flux. RS-based ET estimation algorithms estimate ET using visible to thermal infrared multispectral bands (Li *et al.*, 2012; Pimpale *et al.*, 2015). Satellites or platforms with different remote sensing sensors can provide these multispectral data with different temporal and spatial resolutions (Nigam *et al.*, 2008; Ezenne *et al.*, 2023). The Surface Energy Balance Algorithm for Land (SEBAL) model (Bastiaanssen *et al.*, 1998), the Simplified Surface Energy Balance (SSEB) model (Senay *et al.*, 2011), Surface Energy Balance System (SEBS) model (Su, 2002), Mapping Evapotranspiration at a High Resolution with

Article info - DOI: <https://doi.org/10.54386/jam.v25i3.2254>

Received: 16 June 2023; Accepted: 28 July 2023; Published online : 31 August 2023

"This work is licensed under Creative Common Attribution-Non Commercial-ShareAlike 4.0 International (CC BY-NC-SA 4.0) © Author (s)"

Internalized Calibration (METRIC) model (Allen *et al.*, 2007), Surface Energy Balance Index (SEBI) (Menenti and Choudhury, 1993), Simplified-Surface Energy Balance Index (S-SEBI) (Roerink *et al.*, 2000), and Two Source Energy Balance model (TSEB) (Colaizzi *et al.*, 2012; Norman *et al.*, 1995) are examples of RS-based ET estimation algorithms.

The S-SEBI model initially proposed by Roerink *et al.*, (2000) was extended to map daily ET in such a way that sensible and latent heat fluxes (H and LE) are computed combinedly through the evaporative fraction (Gomez *et al.* 2005; Sobrino *et al.* 2005). In contrast to other methods that attempt to fix the temperature for wet and dry conditions across the entire image, the S-SEBI can estimate the surface energy balance (SEB) by considering its wet and dry conditions. It is also not necessary to have any extra meteorological inputs. Consequently, S-SEBI is relatively straightforward to apply, which makes it suitable for regions lacking in situ data and can generate continuous operational ET products over agricultural areas. The S-SEBI model computes ET from the land surface temperature (Ts) and albedo relationship through evaporative fraction calculation by defining the temperatures in drier and wetter regions.

Despite significant developments in the last few decades, remote sensing-based ET models still face uncertainties, when applied to new environments for which they are not designed or calibrated. As a result, it is constantly a research topic to assess the efficiency of remote sensing-based ET monitoring methods (Chen *et al.*, 2022). The robustness of these RS-based models remains unclear, with the question of whether they can be considered “best” or at least valid under field conditions. We hypothesized that using albedo vs land surface temperature in a trapezoidal space would evolve into a better estimation of ET compared to single values for hot and cold pixels in an image. This is also a simple, straightforward, and less data-intensive method and can be easily adapted for irrigation scheduling in semi-arid farms. This study used S-SEBI to estimate and validate the actual ET spatially using Landsat 8/9 datasets for the two *rabi* seasons.

MATERIALS AND METHODS

Study area

The agricultural farm of the ICAR-Indian Agricultural Research Institute in New Delhi, India (28°7' 22.8" N to 28° 38' 58.92" N and 77° 8' 42.36" to 77°10' 27.84" E) was chosen for the study (Fig. 1). A semiarid climate is characterized by mixed, hyperthermic, Typic Haplustepts soils. Rainfall averages 765.2 mm annually, with 82.5 percent falling between June and September. A total of 242 ha is cropped on the farm during the post-monsoon season, with wheat as the dominant crop (70 percent).

Datasets and processing

The input data in the S-SEBI model include satellite datasets and meteorological data. This study relied on the Eddy Covariance flux tower for input and validation. The satellite images were selected with less than 10% cloud coverage.

Remote sensing datasets

Landsat-8/9 level-2 data (Path 147, 146, and row 40) were downloaded from the United States Geological Survey (USGS) Earth Explorer data portal (<https://earthexplorer.usgs.gov/>) with a spatial resolution of 30 m. Scale factors of 0.0000275 and 0.00341802 with additional offsets of -0.2 and 149.0 per pixel were used to correct the surface reflectance and temperature, respectively. The resolution of the Landsat image was 30 m. We had 12 high-quality images (at least 90% cloud-free) for 2021–2022 and 2022–2023 (Table 1).

S-SEBI model

ET is estimated from remote sensing data by assessing the SEB using surface properties such as albedo, vegetation cover, and Ts. For instantaneous conditions, the SEB is expressed as (Eq. 1):

$$LE = R_n - H - G \quad (1)$$

where R_n , H, and G are the net radiation, sensible heat flux, and soil heat flux, respectively, expressed in W/m^2 , and LE is the latent heat flux which is calculated as

$$LE = EF (R_n - G) \quad (2)$$

where EF is the evaporative fraction which can be calculated as

$$EF = \frac{T_{hot} - T_s}{T_{hot} - T_{cold}} \quad (3)$$

Where T_{hot} and T_{cold} represent the temperature of hot and cold edges, respectively, and T_s is the temperature of the individual pixel (K). The S-SEBI model, T_{hot} and T_{cold} are determined based on the linear regression of T_s and surface albedo (α) (Eq. 4 and 5). The establishment of the linear regression between T_s and albedo and the determination of coefficients were thoroughly explained by Roerink *et al.*, (2000).

$$T_{hot} = a_1 + \alpha b_1 \quad (4)$$

$$T_{cold} = a_2 + \alpha b_2 \quad (5)$$

where α stands for surface albedo; a_1 , a_2 , b_1 and b_2 are the regression coefficients for the dry and wet boundary, respectively. It is important to note that in S-SEBI, T_{cold} represents the cold edge (where $H = 0$), and T_{hot} represents the hot edge where all available energy ($R_n - G$) is assumed equal to H. The hot and cold edges together create a trapezoidal space.

The albedo (α) was calculated using Eq. 6. We used the “Olmedo” coefficient (Olmedo *et al.*, 2016), which are 0.246, 0.146, 0.191, 0.304, 0.105, and 0.008 for Landsat bands 2, 3, 4, 5, 6, and 7.

$$\alpha = \sum W_{band} * r_{band} \quad (6)$$

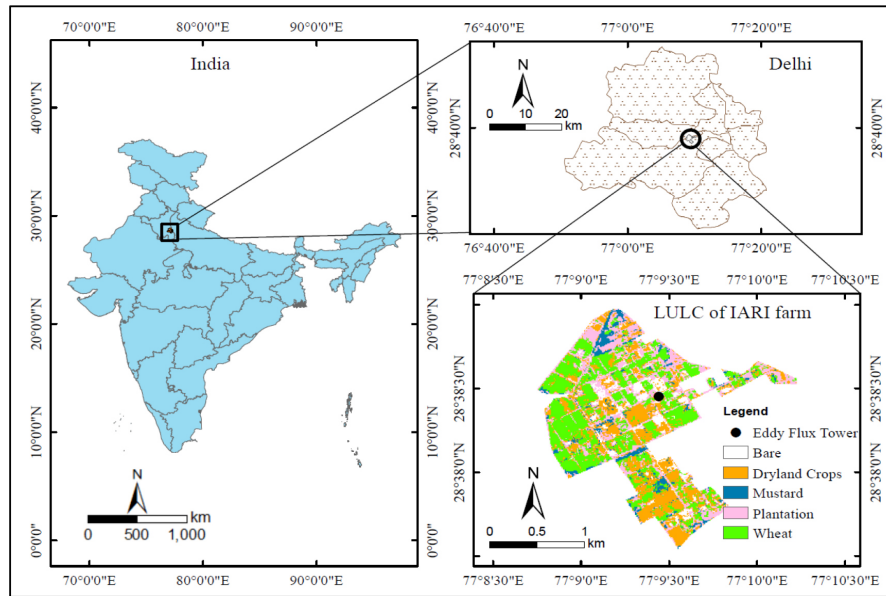


Fig. 1: Study area and land use land cover (LULC) map at ICAR-Indian Agricultural Research Institute (ICAR-IARI), New Delhi, India, during the *rabi* season

Table 1: LANDSAT-8/9 scenes with cloud-free (< 10%) dates were used for estimating ETa

LANDSAT OLI Date of acquisition (DOA)			
<i>Rabi</i> 2021-22	Satellite	<i>Rabi</i> 2022-23	Satellite
November 27, 2021 (331)	L8	November 22, 2022 (326)	L9
December 4, 2021 (338)	L8	November 30, 2022 (334)	L8
December 12, 2021 (346)	L9	December 07, 2022 (341)	L8
December 20, 2021 (354)	L8	December 24, 2022 (358)	L9
January 29, 2022 (29)	L9	January 16, 2022 (16)	L9
February 6, 2022 (37)	L8	February 10, 2022 (41)	L9
February 15, 2022 (46)	L8	February 18, 2022 (49)	L8
March 03, 2022 (62)	L8	February 26, 2022 (57)	L9
March 11, 2022 (70)	L9	March 6, 2022 (65)	L8
March 19, 2022 (78)	L8	March 14, 2022 (73)	L9
March 26, 2022 (85)	L8	March 30, 2022 (89)	L9
April 03, 2022 (93)	L9	April 7, 2022 (97)	L8

N.B: In parentheses, the Day of the Year (DOY) is given, L8 and L9 represent Landsat 8, 9 respectively

W_{band} , and r_{band} are the weight or coefficient, and reflectance for specified bands, respectively.

Net radiation (Rn) is the actual rate of radiant energy received at the earth’s surface, divided into G, H, and LE. It is expressed mathematically as the difference of all incoming radiant fluxes to all outgoing radiant fluxes and is expressed as

$$Rn = (1 - \alpha)Rs \downarrow + RL \downarrow + RL \uparrow + (1 - \epsilon_s)RL \downarrow \quad (7)$$

where $Rs \downarrow$ represents the incoming short-wave radiation (W/m^2), α is the surface short-wave albedo (dimensionless), $RL \downarrow$ and $RL \uparrow$ represent the incoming and outgoing long-wave radiations (W/m^2), and ϵ_s represents the surface emissivity (dimensionless).

$Rs \downarrow$, $RL \downarrow$ and $RL \uparrow$ were computed using standard algorithms described by Allen *et al.*, (2011). The emissivity (ϵ_s) was calculated based on albedo, NDVI, and LAI. If the NDVI < 0 and albedo < 0.47, then $\epsilon_s = 0.99$, else if LAI ≥ 3 , then $\epsilon_s = 0.98$ and if LAI < 3 then $\epsilon_s = 0.97 + (LAI * 0.0033)$. The LAI was calculated using an empirical equation given by Allen *et al.*, (2007) (Eq. 8).

$$LAI = abs\left(-\frac{\ln\left(\frac{0.69 - SAVI}{0.59}\right)}{0.91}\right) \quad (8)$$

Where SAVI represents the soil-adjusted vegetation index (Huete *et al.*, 1988) (dimensionless), which was calculated using the Landsat band 4 (Red) and 5 (NIR) using the following equation

(Eq. 9)

$$SAVI = (1 + L) \frac{(NIR - R)}{NIR + R + L} \quad (9)$$

Where L is a soil correction factor (L= 0.5).

Soil heat flux (G, W/m²) was estimated using a standard empirical equation proposed by Bastiaanssen *et al.*, (1998) (Eq. 10).

$$G = Rn * (Ts - 273.15) (0.0038 + 0.0074\alpha)(1 - 0.98NDVI^4) \quad (10)$$

Where NDVI represents the normalized difference vegetation index (dimensionless) which was calculated using the Landsat band 4 (Red) and 5 (NIR) using the following equation

$$NDVI = (NIR - R) / (NIR + R) \quad (11)$$

Daily ET

The G can be ignored for timescales of one day or longer (such as monthly, seasonal, and yearly). Therefore, actual evapotranspiration (AET, mm/day) at the daily time scale can be estimated using Eq. (12).

$$AET = \frac{86400 * 10^3}{\lambda * \rho_w} EF * Rn \quad (12)$$

Where ρ_w is the density of water (1000 kg/m³), $86,400 * 10^3$ converts metres per second (m/s) to millimetre per day (mm/day), and λ is the latent heat of vaporisation (J/kg). The calculation of λ was done as a function of the surface temperature using the standard procedure described by Allen *et al.*, (2007).

Validation

The model performance was evaluated by comparing the estimated energy balance fluxes with eddy covariance (EC) measurements at the experimental site. A flux tower was installed at the experimental site at (28.63085° N; 88.15733° E) to measure surface fluxes (Fig. 1). EC tower provided ET data at 30-minute intervals that were averaged to calculate daily ET in mm/day.

The agreement between ET measured by EC tower and S-SEBI model was evaluated using correlation coefficient (r), root mean square error (RMSE), mean bias error (MBE), and mean absolute error (MAE).

RESULTS AND DISCUSSION

Weather conditions during the study period

The research was carried out during the *rabi* seasons of 2021-22 and 2022-23. Fig. 2 depicts the meteorological conditions (mean temperature, net radiation, and rainfall) that prevailed during the study period. During the first season (November 20, 2021, to April 15, 2022), the mean daily temperature ranged between 9.6 and 32 °C, net radiation ranged between 32.6 and 226.3 W m⁻², and the

total rainfall was 181.5 mm, 141.3 mm of which fell in January. From November 20, 2022, to April 15, 2023, the average daily temperature varied from 8.2 to 28.7 °C, the net radiation ranged from 36.3 to 231.2 W m⁻², and the total rainfall was 144.5 mm, with 105.4 mm falling in March. There were 13 and 10 rainfall events during the first and second seasons, respectively (Fig. 2).

Relation of land surface temperature (Ts) with air temperature, albedo, and mean ET

As one of the inputs for analyzing land surface processes, including actual and potential evapotranspiration, land surface temperature (Ts) is an integral part of numerous agricultural and ecological studies (Cristóbal *et al.*, 2018). We calculated the mean land surface temperature and ET over the study area by taking the average of all pixels. The mean Ts in relation to the mean ET over the farm is plotted in Fig. 3. Though Ts is influenced by several other factors, like solar energy, and crop cover, the ET_{mean} is closely following the Ts except in November and April 2021 due to the low availability of soil moisture. The soil moisture factor is most noticeable when there is little or no crop cover, which can be well reflected by the variation in Ts (Fig. 3). It is evident that the higher the Ts value, the lower the ET value, as in the maturity stages of the crop development, low soil moisture was prominent in the first season. Still, rainfall increased the soil moisture in the second season, thus increasing ET (Fig. 3). At the initial stage, the mean Ts for seasons 2021-22 and 2022-23 varied from 292.4 K to 299.5 K and 290.44 K to 300.52 K, respectively. We lack cloud-free dates at the crop developmental stage (January) because of western disturbance. At the mid-season stage (Feb – 15th March), the average LST was 299.1 K and 303.5 K for 2021-22 and 2022-23, respectively. The low mean Ts on 12 and 20th Dec, 2021 and 29th January 2022 could be attributed to low air temperature. Similarly, in 2022-23 there was a sudden drop in Ts on 24th December 2022, and 16th January 2023 might be due to low air temperature and net radiation compared to preceding and succeeding dates (Fig. 3). Our study found a good correlation (R² = 0.92) between mean air temperature (T_{air}) and Ts (Fig. 4). Goldblatt *et al.*, (2021) also reported a significant correlation (r = 0.45, p < 0.001) between LST and mean air temperature.

The hot edge (T_{hot}) and cold edge (T_{cold}) were calculated from the trapezoidal space plot between albedo and Ts, as suggested by Roerink *et al.*, (2000), for all satellite overpass dates. A representative trapezoidal space plot for estimating T_{hot} and T_{cold} as a linear function of surface albedo for the study region is shown in Fig. 5. The slope and intercept of the hot and cold edges, as well as the coefficient of determination (R²) of the regression line, for all satellite overpass dates, are listed in Table 2.

Spatially and seasonally distributed ET

ET products can be more efficiently retrieved at the farm scale using remote sensing techniques that are spatially consistent and temporally continuous. This methodology has the advantage of providing estimates across the entire territory, capturing minor spatial variations between pixels that allow one to assess water use, irrigation, and groundwater recharge efficiency (Khan *et al.*, 2020). The model performance at a spatiotemporal scale on a pixel-

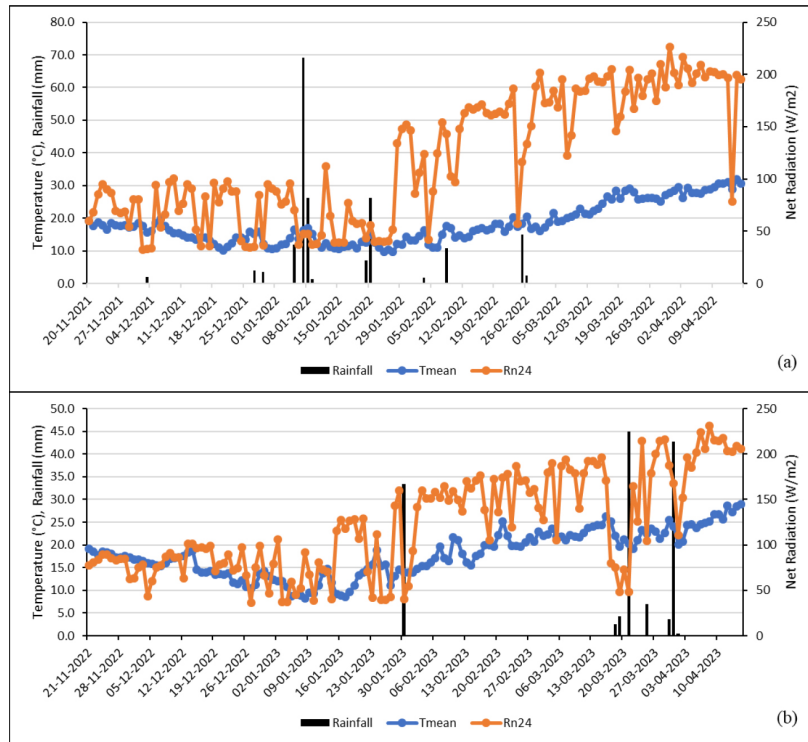


Fig. 2: Daily weather [mean temperature (Tmean), net radiation (Rn24), and rainfall] over the crop growing season (a) Rabi 2021-22, (b) 2022-23

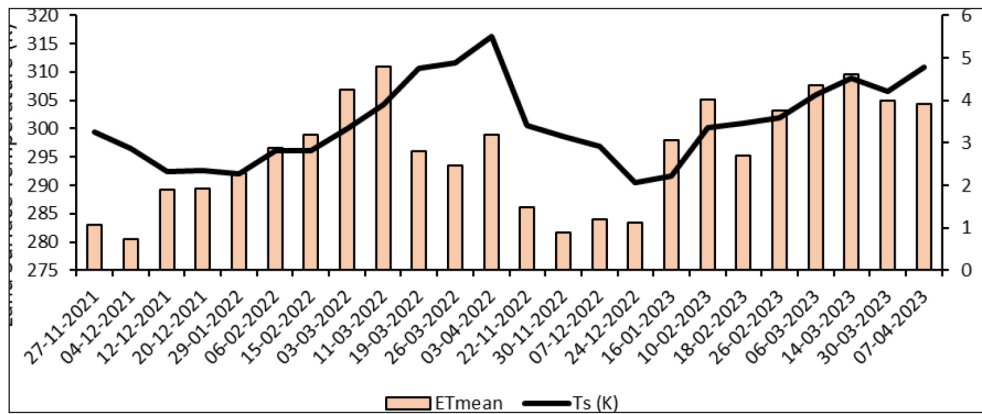


Fig. 3: Variation of mean land surface temperature and mean ET over the IARI farm on satellite overpass dates.

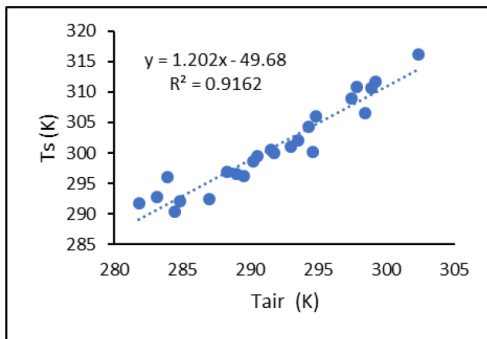


Fig. 4: Relation between mean air temperature (Tair) and mean land surface temperature (Ts)

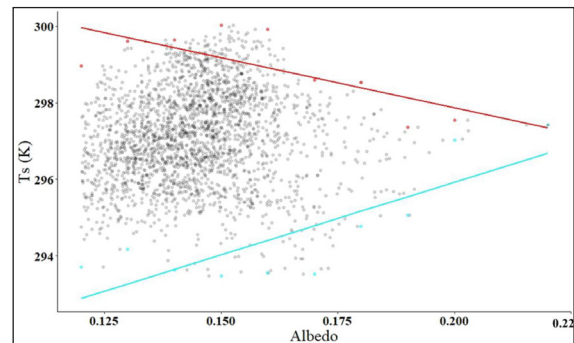


Fig. 5: Relationship between albedo and land surface temperature (Date: 07.12.2022), the red line represents the hot edge, and the blue line represents the cold edge.

Table 2: Slope and intercept of hot and cold edge and R²

Date	T _{hot}		R ²	T _{cold}		R ²
	Slope	Intercept		Slope	Intercept	
27-11-2021	-7.581	302.847	0.039	17.743	294.804	0.604
04-12-2021	-21.129	305.838	0.748	23.253	292.761	0.576
12-12-2021	-39.656	300.815	0.707	21.012	286.751	0.869
20-12-2021	-35.656	301.534	0.812	24.446	286.459	0.639
29-01-2022	-7.991	295.418	0.081	27.139	286.643	0.632
06-02-2022	-6.427	297.503	0.022	31.753	287.197	0.615
15-02-2022	-8.242	303.100	0.035	26.581	292.818	0.588
03-03-2022	-18.930	308.970	0.182	23.151	296.569	0.836
11-03-2022	-12.503	310.953	0.064	38.389	295.889	0.857
19-03-2022	11.341	313.417	0.065	29.717	303.899	0.741
26-03-2022	10.660	314.820	0.076	54.834	299.561	0.879
03-04-2022	30.892	316.016	0.580	99.855	297.621	0.778
22-11-2022	-8.861	305.058	0.042	15.795	295.286	0.659
30-11-2022	-19.831	304.104	0.205	30.096	291.435	0.517
07-12-2022	-30.125	304.044	0.702	33.532	288.963	0.604
24-12-2022	-18.391	295.304	0.411	35.991	282.852	0.788
16-01-2022	-36.024	300.737	0.811	33.290	284.475	0.852
10-02-2023	-21.101	306.506	0.383	32.953	292.843	0.873
18-02-2023	-26.114	308.201	0.574	36.659	293.359	0.862
26-02-2023	-11.394	306.570	0.145	39.244	293.913	0.910
06-03-2023	-9.979	311.145	0.202	38.899	297.204	0.899
14-03-2023	4.137	312.446	0.011	47.897	298.305	0.748
30-03-2023	-4.299	309.078	0.045	16.232	302.167	0.489
07-04-2023	17.635	311.994	0.252	28.693	303.223	0.869

by-pixel basis over heterogeneous land cover was assessed through the S-SEBI generated maps. Fig. 6 depicts the spatial pattern of daily ET obtained from the S-SEBI method using Landsat 8/9 image over the IARI farm during the *rabi* seasons of 2021-22 and 2022-23. Overall, the S-SEBI model can capture the spatiotemporal variability of the atmosphere's evaporative demand over the entire study area. In general, the spatiotemporal patterns of ET can be highly variable due to the heterogeneity of land surface and environmental factors that control ET (Sharma *et al.*, 2015). There was a significant spatiotemporal variation in ET in the study area due to the variability in sowing times, cropping systems, and agronomic practices. The model could distinguish the ET over dryland crops and well-irrigated wheat fields over the IARI farm (Fig. 1, 6). The model estimated mean ET over the farm at the initial crop growing stage (Nov-Dec) varied between 0.73 (December 4, 2021) and 1.92 (December 20, 2021) mm/day for the first season and the second season it ranged from 0.89 (Nov 30, 2022) to 1.48 (Nov 22, 2021) mm/day (Fig. 6). In the mid-season stage (February-mid March), ET values ranged from 2.88 to 4.79 mm/day and 2.7 to 4.62 mm/day for the first and second seasons, respectively. However, in April, the mean ET was 3.27 mm/day for the first season, while it was relatively high (3.92 mm/day) for the second season due to the high soil moisture content from heavy rainfall. With the higher air temperature and abundant solar radiation during mid-season (Feb-Mar), the from a well-watered surface due to the greater availability

of energy (French *et al.*, 2020).

Table 3: Season-wise and overall model performance matrices

Statistical Parameter	2021-22	2022-23	Overall
r	0.905	0.904	0.894
MBE (mm/day)	0.595	0.2	0.398
MAE (mm/day)	0.821	0.499	0.66
RMSE (mm/day)	0.975	0.558	0.794

Comparison of S-SEBI estimated and eddy covariance measured ET

The various statistical parameters were considered for the quantitative evaluation of model performance. During 2021-22, the correlation coefficient (r) was 0.905, the MBE was 0.595 mm/day, the MAE was 0.821, and the RMSE was 0.975 mm/day. In 2022-23, the correlation coefficient (r) was 0.904, and the MBE, MAE, and RMSE were 0.2, 0.499, and 0.558 mm/day, respectively. (Fig. 7, Table 3). In the study, it has been found that the model tends to overestimate at higher ET values and underestimate at lower ET values (Fig. 7). We observed an overall correlation coefficient of 0.894 and an RMSE of 0.794 mm/day for model-estimated ET. Danodia *et al.*, (2017) also found a close relationship between S-SEBI derived and scintillometer-observed evaporative fractions with a correlation coefficient of 0.85. Sobrino *et al.*, (2021) reported that an average RMSE for daily ET of 0.86 mm/day was obtained

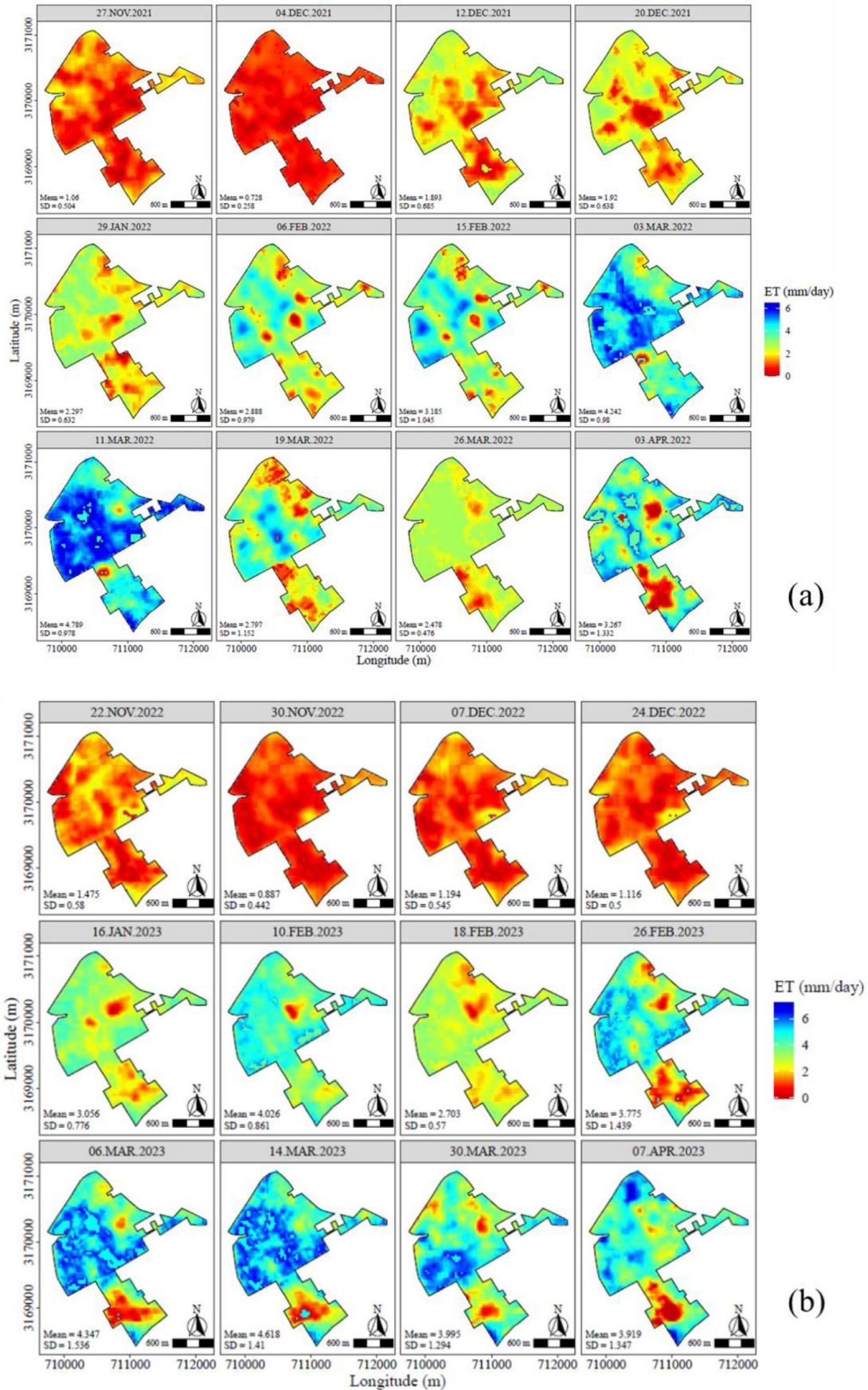


Fig. 6: Spatial variation of ET over the IARI farm (a) Rabi 2021-22, (b) Rabi 2022-23

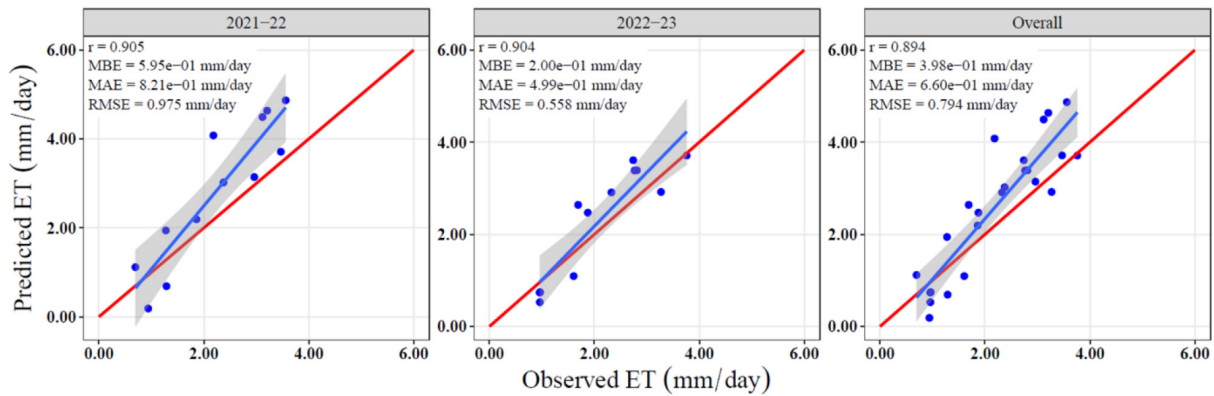


Fig. 7: Relationship between the estimated ET and the eddy flux ET for both the season and overall

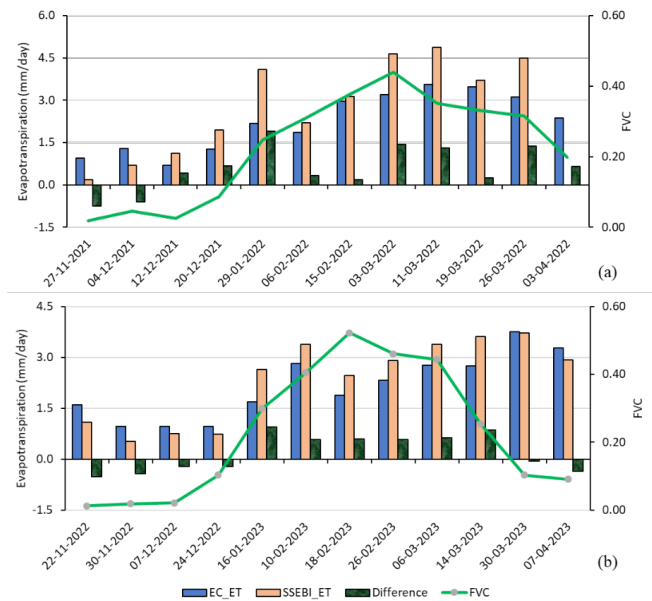


Fig. 8: Observed (eddy covariance flux tower ET), S-SEBI model predicted ET, difference, and fractional vegetation cover (FVC) on satellite overpass dates for both crop growing seasons (a) Rabi 2021-22, (b) Rabi 2022-23

from the S-SEBI model for Landsat 8 data. At the initial stage, the model estimated ET ranged from 0.69 to 1.94 and 0.527 to 1.09 mm/day for the first and second seasons, respectively. At the mid-season stage, ET ranged from 2.19 to 4.87 mm/day for the first season and from 2.47 to 3.6 mm/day for the second season. Mukherjee *et al.*, (2021) estimated actual ET using Operational Simplified Surface Energy Balance and found that the ET ranged from 0.81 to 3.26 mm/day during the initial stage and 1.83 to 4.02 mm/day at the mid-season. At the initial crop developmental stage, the model tends to underestimate by an average of 0.48 mm/day and 0.76 mm/day for the first and second seasons, respectively. Moreover, compared to the initial crop growth stage, the development stages showed higher ET (Fig. 8). As a result of a smaller canopy cover of the crop during its initial growth stage, there may be less solar radiation captured by the crop, leading to smaller sensible and latent heat fluxes than during the development stages (Kumar *et al.*, 2019). An average 0.73 mm/day overestimation of daily ET by S-SEBI (Fig. 7) implies

that the Ts vs. albedo relationship utilized in the S-SEBI model to determine the wet edge and dry edge may not be well represented over the farm. A similar overestimation of S-SEBI-estimated ET (16%) was observed by Wagle *et al.* (2017) in Oklahoma.

CONCLUSIONS

Our study analyzed the operational ET data obtained through the S-SEBI model from Landsat 8/9 data during the post-monsoon periods of 2021-22 and 2022-23. After extensive analysis, we found that the S-SEBI model has an overall correlation coefficient of 0.89 and an RMSE of 0.79 mm/day for ET. Based on these results, we highly recommend the S-SEBI model as a simple yet effective tool for mapping daily ET over agricultural sites. This data can be used for remote sensing-based crop irrigation scheduling, providing valuable insights for farmers.

ACKNOWLEDGMENTS

The authors thank the Director, ICAR-IARI, New Delhi, and ICAR-National Fellow project for providing the necessary facilities and funding for carrying out the research work to complete the Ph.D. thesis.

Conflict of interest statement: The authors declare that they have no conflict of interest.

Data availability statement: The data analyzed in this study is subject to the following licenses/restrictions. Our Institute does not allow sharing of data publicly.

Author contribution statement: **T. Ghosh:** Conceptualization, Methodology, Writing – original draft, Writing – review & editing, Data Analysis, Data Curation; **D. Chakraborty:** Conceptualization, Methodology, Writing – original draft, Writing – review & editing; **B. Das:** Conceptualization, Methodology, Writing – original draft, Writing – review & editing, Data Analysis; **V. K. Sehgal:** Conceptualization, Methodology; **D. Roy:** Data Analysis; **J. Mukherjee:** Conceptualization, Methodology, **R. Dhakar:** Conceptualization, Methodology, Data Analysis; **K. Bag:** Data Analysis, Data Curation.

Disclaimer: The opinions, contents, and views expressed in the research article published in the Journal of Agrometeorology are the authors' own and do not necessarily reflect the position of the

organizations they are affiliated with.

Publisher's Note: The periodical remains neutral with regard to jurisdictional claims in published maps and institutional affiliations.

REFERENCES

- Allen, R.G., Tasumi, M. and Trezza, R. (2007). Satellite-based energy balance for mapping evapotranspiration with internalized calibration (METRIC)—Model. *J. Irrig. Drain. Eng.*, 133(4): 380-394. [https://doi.org/10.1061/\(ASCE\)0733-9437\(2007\)133:4\(380\)](https://doi.org/10.1061/(ASCE)0733-9437(2007)133:4(380))
- Allen, R.G., Pereira, L.S., Howell, T.A. and Jensen, M.E. (2011). Evapotranspiration information reporting: II. Recommended documentation. *Agric. Water Manage.*, 98(6): 921-929. <https://doi.org/10.1016/j.agwat.2010.12.016>
- Bag, K., Bandyopadhyay, K.K., Sehgal, V.K., Sarangi, A. and Krishnan, P. (2020). Effect of tillage, residue and nitrogen management on radiation interception, radiation use efficiency and evapotranspiration partitioning. *J. Agrometeorol.*, 22(3): 285-294. DOI: <https://doi.org/10.54386/jam.v22i3.190>
- Chattopadhyay, N., Vyas, S.S., Bhattacharya, B.K. and Chandras, S. (2016). Evaluating the potential of rainfall product from Indian geostationary satellite for operational agromet advisory services in India. *J. Agrometeorol.*, 18(1): 29-33. DOI: <https://doi.org/10.54386/jam.v18i1.895>
- Bastiaanssen, W.G., Menenti, M., Feddes, R.A., and Holtslag, A.A.M. (1998). A remote sensing surface energy balance algorithm for land (SEBAL). 1. Formulation. *J. Hydrol.*, 212: 198-212. DOI: [https://doi.org/10.1016/S0022-1694\(98\)00253-4](https://doi.org/10.1016/S0022-1694(98)00253-4)
- Boretti, A. and Rosa, L. (2019). Reassessing the projections of the world water development report. *NPJ Clean Water.*, 2(1): 15. DOI: <https://doi.org/10.1038/s41545-019-0039-9>
- Chen, H., Zhu, G., Shang, S., Qin, W., Zhang, Y., Su, Y., and Xu, C. (2022). Uncertainties in partitioning evapotranspiration by two remote sensing-based models. *J. Hydrol.*, 604: 127223. DOI: <https://doi.org/10.1016/j.jhydrol.2021.127223>
- Cleverly, J., Thibault, J.R., Teet, S.B., Tashjian, P., Hipps, L.E., Dahm, C.N., and Eamus, D. (2015). Flooding regime impacts on radiation, evapotranspiration, and latent energy fluxes over groundwater-dependent riparian cottonwood and saltcedar forests. *Adv. Meteorol.*, 2015. DOI: <https://doi.org/10.1155/2015/935060>
- Colaizzi, P.D., Kustas, W.P., Anderson, M.C., Agam, N., Tolch, J.A., Evett, S.R. and O'Shaughnessy, S. A. (2012). Two-source energy balance model estimates of evapotranspiration using component and composite surface temperatures. *Adv. Water Resour.*, 50: 134-151. DOI: <https://doi.org/10.1016/j.advwatres.2012.06.004>
- Cristóbal, J., Jiménez-Muñoz, J.C., Prakash, A., Mattar, C., Skoković, D. and Sobrino, J.A. (2018). An improved single-channel method to retrieve land surface temperature from the Landsat-8 thermal band. *Remote Sens.*, 10(3): 431. DOI: <https://doi.org/10.3390/rs10030431>
- Danodia, A., Patel, N.R., Chol, C.W., Nikam, B.R. and Sehgal, V.K. (2019). Application of S-SEBI model for crop evapotranspiration using Landsat-8 data over parts of North India. *Geocarto Int.* 34, (1): 114-131. DOI: <https://doi.org/10.1080/10106049.2017.1374473>
- Ezenne, G.I., Eyibio, N.U., Tanner, J.L., Asoiro, F.U. and Obalum, S.E. (2023). An overview of uncertainties in evapotranspiration estimation techniques. *J. Agrometeorol.*, 25(1): 173-182. DOI: <https://doi.org/10.54386/jam.v25i1.2014>
- French, A.N., Hunsaker, D.J., Sanchez, C.A., Saber, M., Gonzalez, J.R. and Anderson, R. (2020). Satellite-based NDVI crop coefficients and evapotranspiration with eddy covariance validation for multiple durum wheat fields in the US Southwest. *Agric. Water Manage.*, 239: 106266. DOI: <https://doi.org/10.1016/j.agwat.2020.106266>
- Goldblatt, R., Addas, A., Crull, D., Maghrabi, A., Levin, G.G. and Rubinyi, S. (2021). Remotely sensed derived land surface temperature (LST) as a proxy for air temperature and thermal comfort at a small geographical scale. *Land*, 10(4): 410. DOI: <https://doi.org/10.3390/land10040410>
- Gomez, M., Olioso, A., Sobrino, J.A. and Jacob, F. (2005). Retrieval of evapotranspiration over the Alpilles/ReSeDA experimental site using airborne POLDER sensor and a thermal camera. *Remote Sens. Environ.*, 96(3-4): 399-408. DOI: <https://doi.org/10.1016/j.rse.2005.03.006>
- Huete, A.R. (1988). A soil-adjusted vegetation index (SAVI). *Remote Sens. Environ.*, 25(3): 295-309. DOI: [https://doi.org/10.1016/0034-4257\(88\)90106-X](https://doi.org/10.1016/0034-4257(88)90106-X)
- Jin, Y., He, R., Marino, G., Whiting, M., Kent, E., Sanden, B.L., Culumber, M., Ferguson, L., Little, C., Grattan, S., Tha Paw U, K., Lagos, Luis O., Snyder R. and Zaccaria, D. (2018). Spatially variable evapotranspiration over salt affected pistachio orchards analyzed with satellite remote sensing estimates. *Agric. For. Meteorol.*, 262: 178-191. DOI: <https://doi.org/10.1016/j.agrformet.2018.07.004>
- Khan, M.S., Baik, J. and Choi, M. (2020). Inter-comparison of evapotranspiration datasets over heterogeneous landscapes across Australia. *Adv. Space Res.*, 66(3): 533-545. DOI: <https://doi.org/10.1016/j.asr.2020.04.037>
- Kisekka, I., Peddinti, S.R., Kustas, W.P., McElrone, A.J., Bambach-Ortiz, N., McKee, L. and Bastiaanssen, W. (2022). Spatial-temporal modeling of root zone soil moisture dynamics in a vineyard using machine learning and remote sensing. *Irrig. Sci.*, 40(4-5): 761-777. DOI: <https://doi.org/10.1007/s00271-022-00775-1>

- Li, Z., Zheng, F.L., and Liu, W.Z. (2012). Spatiotemporal characteristics of reference evapotranspiration during 1961–2009 and its projected changes during 2011–2099 on the Loess Plateau of China. *Agric. For. Meteorol.*, 154 (2012): 147-155. DOI: <https://doi.org/10.1016/j.agrformet.2011.10.019>
- Menenti, M. and Choudhury, B. (1993). Parameterization of Land Surface Evapotranspiration Using a Location Dependent Potential Evapotranspiration and Surface Temperature Range. Exchange Processes at the Land Surface for a Range of Space and Time Scales, *IAHS Publication*, 212: 561-568.
- Mukherjee, J., Sharma, A., Dhakar, R., Sehgal, V.K., Chakraborty, D. and Das, D.K. (2021). Estimation and Validation of Actual Evapotranspiration (ET a) of Maize Wheat Cropping System Using SSEBop Model Over IARI Research Farm, New Delhi, India. *J. Indian Soc. Remote Sens.*, 49: 1823-1837. DOI: <https://doi.org/10.1007/s12524-021-01350-5>
- Nigam, R., Mallick, K., Bhattacharya, B.K., Pandey, V. and Patel, N.K. (2008). Heat flux estimation from MODIS TERRA-AQUA and validation over a semi-arid agroecosystem using scintillometry and model simulation. *J. Agrometeorol*, 10 (special issue-Part I), 75:81.
- Norman, J.M., Kustas, W.P. and Humes, K.S. (1995). Source approach for estimating soil and vegetation energy fluxes in observations of directional radiometric surface temperature. *Agric. For. Meteorol.*, 77(3-4): 263-293. DOI: [https://doi.org/10.1016/0168-1923\(95\)02265-Y](https://doi.org/10.1016/0168-1923(95)02265-Y)
- Olmedo, G.F., Ortega Farias, S., Fonseca Luengo, D., and Fuentes Peñailillo, F. (2016). Water: tools and functions to estimate actual evapotranspiration using Land Surface Energy Balance Models in R.
- Parmar, H.V. and Gontia, N.K. (2016). Remote sensing based vegetation indices and crop coefficient relationship for estimation of crop evapotranspiration in Ozat-II canal command. *J. Agrometeorol*, 18(1): 137-140. DOI: <https://doi.org/10.54386/jam.v18i1.918>
- Pimpale, A.R., Rajankar, P.B., Wadkatkar, S.B., Wanjari, S.S. and Ramteke, I.K. (2015). Estimation of water requirement of wheat using multispectral vegetation indices. *J. Agrometeorol*, 17(2): 208-212. DOI: <https://doi.org/10.54386/jam.v17i2.1008>
- Roerink, G.J., Su, Z. and Menenti, M. (2000). S-SEBI: A simple remote sensing algorithm to estimate the surface energy balance. *Phys. Chem. Earth Part B*, 25(2), 147-157. DOI: [https://doi.org/10.1016/S1464-1909\(99\)00128-8](https://doi.org/10.1016/S1464-1909(99)00128-8)
- Senay, G.B., Budde, M.E. and Verdin, J.P. (2011). Enhancing the Simplified Surface Energy Balance (SSEB) approach for estimating landscape ET: Validation with the METRIC model. *Agric. Water Manage.*, 98(4): 606-618. DOI: <https://doi.org/10.1016/j.agwat.2010.10.014>
- Sharma, V., Irmak, S., Kilic, A. and Mutiibwa, D. (2015). Application of remote sensing for quantifying and mapping surface energy fluxes in south central Nebraska: Analyses with respect to field measurements. *Trans. ASABE*, 58(5): 1265-1285. DOI: <https://doi.org/10.13031/trans.58.11091>
- Sholihah, R., Dasanto, B.D. and Hendarti, H. (2016). Water allocation plan on part of Cisadane catchment in the district and city of Bogor. *J. Tek. Hidraulik*, 7(2): 195-210. DOI: <https://doi.org/10.32679/jth.v7i2.568>
- Sobrino, J.A., Gómez, M., Jiménez-Muñoz, J.C., Olioso, A. and Chehbouni, G. (2005). A simple algorithm to estimate evapotranspiration from DAIS data: Application to the DAISEX campaigns. *J. Hydrol.*, 315(1-4): 117-125. DOI: <https://doi.org/10.1016/j.jhydrol.2005.03.027>
- Sobrino, J.A., Souza da Rocha, N., Skoković, D., Suélen Käfer, P., López-Urrea, R., Jiménez-Muñoz, J. C. and Alves Rolim, S. B. (2021). Evapotranspiration Estimation with the S-SEBI Method from Landsat 8 Data against Lysimeter Measurements at the Barrax Site, Spain. *Remote Sens.*, 13(18): 3686. DOI: <https://doi.org/10.3390/rs13183686>
- Su, Z. (2002). The Surface Energy Balance System (SEBS) for estimation of turbulent heat fluxes. *Hydrol. Earth Syst. Sci.*, 6(1): 85-100. DOI: <https://doi.org/10.5194/hess-6-85-2002>